J. Fluid Mech. (1984), *vol.* 149, *pp.* 71–88
Printed in Great Britain

Starting flow for an obstacle moving transversely in a rapidly rotating fluid

By E. R. JOHNSON
Department of Mathematics, University College London, Gower Street, London WC1E 6BT

(Received 1 December 1983)

The initial-value problem for Taylor columns is considered for the oceanographically relevant case of slow flow over obstacles of small slope, and horizontal scale of order of the fluid depth or larger. In such flows depth variations cause, in the neighbourhood of the obstacle, a gradient of background potential vorticity. Topographic Rossby waves, forced in the starting flow, propagate across the gradient, cycling the obstacle in times of order of the topographic vortex-stretching time $h/2\Omega h_0$, where h is the fluid depth, Ω the background rotation rate and h_0 the obstacle height. The linear inertial-wave equation and the quasigeostrophic equations are related by considering the case where the inertial period is small compared with the topographic time, which is in turn small compared with the advection time.

When viscosity is present the waves decay to a steady motion in a time of order of the viscous spin-up time. In inviscid flow the waves do not decay. The flow oscillates about steady, irrotational, zero-circulation flow. The drag and lift on the obstacle oscillate with almost constant frequency and amplitude equal to the Coriolis force on a body of fluid whose volume matches that of the obstacle. Particles above a right cylinder move in closed orbits of diameter $1/S$, where S is the topographic parameter introduced by Hide (1961). Particles away from the cylinder move irrotationally, but asymmetrically, from upstream to downstream. A shear layer is present at the boundary of the cylinder throughout the motion. The initial vorticity distribution for flow over a paraboloid is everywhere finite. However, regions of positive and negative vorticity interlace ever more closely during the motion, causing at large time a similar shear layer at the column boundary. By this time the vorticity is increasing without bound above the obstacle and neglected nonlinear, horizontal viscous, or vertical effects are important.

1. Introduction

The Taylor–Proudman theorem states that slow, steady perturbations to an incompressible inviscid fluid that would otherwise be in rapid solid-body rotation are independent of distance along the axis of rotation. In his well-known experiment Taylor (1923) demonstrated the remarkable flow forced when a short cylinder is set into slow steady motion across the base of a rapidly rotating tank of water: the flow pattern appears independent of depth even though the forcing is of limited vertical extent. The theory and experiments for this and similar flows are of increasing interest owing to their relevance to topographic forcing of large-scale ocean flows. It is the purpose of the present work to investigate the starting problem for such flows in the light of recent numerical work (James 1980) showing the possibility of large oscillations in the force on obstacles set in motion in shallow, rapidly rotating flows.

The Taylor–Proudman theorem does not predict the flow pattern. Grace (1927)

restored the time-dependent terms and attempted to find the final state of the motion by expanding quantities as a power series in time. This approach is used in §5 of the present paper to discuss the initial development of the flow, but is inherently unsatisfactory for the long-term behaviour. Stewartson (1953) completed Grace's analysis for motion of an ellipsoid in an inifinite fluid, but found little agreement with experiment and an unsatisfactory prediction of non-zero velocities at infinity. Stewartson (1967) pointed out the importance of the finite vertical extent of the fluid in determining the final state of the flow, and calculated the motion including the effect of rigid horizontal boundaries. For flow depths large, but of the same order as obstacle dimensions,† he obtained a flow pattern consisting of a stagnant vertical cylindrical column circumscribing a sphere and irrotational steady flow with zero circulation round the cylinder (e.g. Batchelor 1967, figure 6.6.1*a*). The disparate regions are matched by a time-dependent vertical shear layer. Stewartson noted that the solution agrees with the highly viscous steady solution of Jacobs (1964) but does not possess the asymmetry about the cylinder in the cross-stream direction observed in experiments.

An alternative approach consists of considering nonlinear effects in steady, shallow, quasigeostrophic flow and the conservation of potential vorticity (Hide 1961; Ingersoll 1969; Huppert 1975). Ingersoll (1969) obtained unique solutions with a stagnant column partially covering a right circular cylinder by requiring Ekman pumping to spin down any closed streamline region to become stagnant. The flow has non-zero vorticity above the obstacle outside the Taylor-column region and hence non-zero circulation about the obstacle. These solutions display the asymmetry observed in experiments. As the flow velocity decreases – the limit in which the nonlinear solutions should approach the linear zero-circulation solution of Jacobs (1964) and Stewartson (1967) – the circulation approaches a non-zero constant. The limit of Ingersoll's solution is again a stagnant column circumscribing the cylinder with two-dimensional irrotational flow outside. In this case, however, the flow has exactly the circulation to give a single stagnation point on the column boundary (e.g. Batchelor 1967, figure 6.6.1 (*c*), with flow direction reversed). This point is considered again in §6.

Further information on flow development comes from numerical integration of the initial-value problem for the nonlinear equations. Huppert & Bryan (1976) presented integrations for stratified flow and James (1980) for the simpler equations of quasigeostrophic homogeneous flow. The compression of vortex lines on the upstream side of an obstacle and their extension on the downstream side lead to the formation of an upstream region of negative relative vorticity and a downstream region of positive relative vorticity. Provided the oncoming flow is sufficiently slow, the two areas remain close to the obstacle and move clockwise round the topography. Owing to the large horizontal diffusivities in Huppert & Bryan's calculations, the patches of vorticity appear to stabilize in a position across the flow with the positive vortex to the right looking downstream. Steady solutions of the inviscid nonlinear equations demonstrating this behaviour were obtained by a variational characterization in Johnson (1978). Lower horizontal viscosity in James' model means that his solutions are unsteady until Ekman pumping dissipates any shed eddy.

† The problem of obstacles in very deep rotating flows (where the horizontal scale is of higher order, in some small parameter measuring nonlinearity or viscosity, than the fluid depth) remains of interest both experimentally (Hide, Ibbetson & Lighthill 1968) and theoretically (Cheng 1977; Stewartson & Cheng 1979; Mason & Sykes 1981; Johnson 1982; Cheng & Johnson 1982), but is not directly relevant to topographic forcing of oceanographic flows.

The present work considers a simplified equation, susceptible to analytic treatment, for the temporal development of both viscous and inviscid flows in the presence of strong topographic effects. The fractional change in length, δ say, in vertical vortex lines passing over an obstacle introduces relative vorticity of magnitude of order $2\Omega\delta$, where Ω is the basic rotation rate of the flow. This introduces a topographic vortex-stretching timescale of order $(2\Omega\delta)^{-1}$ that measures the time taken for a topographic Rossby to cycle round the obstacle perpendicular to the gradient of background potential vorticity introduced by the obstacle slope. In §2 the timescale of the flow is chosen to be the topographic time, taken to be long compared with the inertial period (by considering obstacles of small slope in the inertial-wave problem) but short compared with the advection time (by considering strong topographic effects in the potential-vorticity equation). In this limit the equations reduce to a nonlinear viscous system whose inviscid linear wavelike solutions are related to those discussed by Rhines (1969) and whose viscous, steady, linear solutions are discussed by Hickie (1972). In §3 the initial-value problem for those flows is formulated for axisymmetric obstacles and reduced to the solution of an ordinary differential equation by introduction of the Laplace transform.

The solution for a right-circular cylinder is given in §4. The cylinder walls have infinite slope, and so the small-slope limit is not valid near them. The cylinder, however, may be regarded as the limit of steep-sided obstacles, and the solution is presented briefly as it has many of the features of solutions for smoother shapes, yet can be expressed in a simple closed form. The start-up flow forces a single topographic wave of azimuthal wavenumber unity that cycles clockwise round the cylinder. The force on the cylinder consists of a constant cross-stream lift component and a component whose direction rotates with angular velocity $\frac{1}{2}$. In viscous flow the wave motion and rotating force component decay on a timescale of order of the viscous spin-up time. The frequency and decay rate model those obtained numerically by James (1980). Inviscid motion does not decay. The streamline pattern is periodic. The drag and lift oscillate at fixed frequency and amplitude equal to the Coriolis force exerted on a body of fluid whose volume matches that of the cylinder. They are thus non-zero in the limit $S^{-1} \to 0$ (where $S \gg 1$ is the Hide (1961) topographic parameter). The flow oscillates irrotationally with amplitude S^{-1} about the Stewartson (1967) solution. Particles initially above the cylinder move in circular orbits of radius $2S^{-1}$, and those introduced upstream pass downstream following paths that are order-S^{-1} perturbations about steady zero-circulation flow past a right cylinder. Dye visualizations of the flow at large S would show an almost fixed dyed region above the cylinder separated from dye lines stretching from upstream to downstream infinity even though the particles above the cylinder were not at rest and the forces on the cylinder were varying rapidly with significant amplitude. The vorticity of the flow is concentrated in two sheets at the boundary of the cylinder – one fixed and one rotating with the topographic wave period.

A more realistic description of the vorticity-field development follows from the solution in §5 for flow over a paraboloid. The start-up flow forces above the obstacle a set of viscously damped topographic waves of azimuthal wavenumber unity. These in turn force an unsteady irrotational flow away from the obstacle. The streamline pattern, particle paths and force components oscillate almost periodically with period of the lowest mode present, the flow behaviour closely mirroring the simpler flow above a cylinder. The distributions of positive and negative vorticity, formed in the initial stages of the flow, spiral clockwise inwards towards the centre of the paraboloid, intertwining and decaying by an amount depending on the viscosity of the

flow. The linear solution for inviscid flow shows the spirals intertwining increasingly and vorticity everywhere growing in magnitude without limit. The long-term behaviour is determined by neglected vertical variations, horizontal diffusion or nonlinearity. Some comments on these effects and the applicability of these results to more general flows and obstacle shapes are given in §6.

2. Governing equations

Consider an obstacle of horizontal lengthscale l and height h_0 on the lower boundary of an incompressible fluid of constant density ρ and kinematic viscosity ν, and depth h, confined between two horizontal planes and rotating as a rigid body with angular frequency Ω about a vertical axis. Suppose that at time $t^* = 0$ the obstacle is set in motion along the boundary in a straight line with constant speed U such that the Rossby number $Ro = U/2\Omega l$ is small. Take Cartesian axes $Ox^*y^*z^*$ with origin fixed within the obstacle, Ox^* in the opposite direction to the motion of the obstacle and Oz^* vertical. Let the corresponding velocity components be (u^*, v^*, w^*) and introduce the non-dimensional variables

$$\left.\begin{aligned} x &= \frac{x^*}{l}, \quad y = \frac{y^*}{l}, \quad z = \frac{z^*}{h}, \quad \tau = \frac{t^*U}{l}, \\ u &= \frac{u^*}{U}, \quad v = \frac{v^*}{U}, \quad w = \frac{w^*l}{Uh_0}, \quad p = \frac{p^*-p_e^*}{2\Omega\rho Ul}, \end{aligned}\right\} \tag{2.1}$$

where $p^* - p_e^*$ gives the deviation of the pressure from its equilibrium value. The scale for t^* has been taken as the advection time and that for w^* as the vertical velocity forced at the lower boundary by the motion of the obstacle. The flow depends on three non-dimensional parameters other than the Rossby number. These may be taken as the aspect ratio $\lambda = l/h$ of the motion, an Ekman number $E = \nu/2\Omega l^2$ and the fractional depth $\delta = h_0/h$ occupied by the obstacle. In terms of these parameters the equations of motion are

$$Ro\,\mathrm{D}_t u - v = -p_x + E\nabla^2 u, \quad Ro\,\mathrm{D}_t v + u = -p_y + E\nabla^2 v, \tag{2.2a, b}$$

$$Ro\,\mathrm{D}_t w = -\lambda^2 p_z + E\delta\nabla^2 w, \quad u_x + v_y + \delta w_z = 0, \tag{2.2c, d}$$

where $\mathrm{D}_t = \partial_\tau + u\,\partial_x + v\,\partial_y + \delta w\,\partial_z$ and $\nabla^2 = \partial_x^2 + \partial_y^2 + \lambda^2\partial_z^2 = \nabla_1^2 + \lambda^2\partial_z^2$.

The initial conditions and far-field conditions give

$$u = v = w = 0 \quad \text{at} \quad \tau = 0 \quad \text{for each } x, y, \tag{2.3a}$$

$$(u, v, w) \to (1, 0, 0) \quad \text{as} \quad x^2 + y^2 \to \infty \quad \text{for} \quad \tau > 0. \tag{2.3b}$$

For a viscous fluid both the normal and tangential components of velocity vanish at solid boundaries. In rapidly rotating flows where $Ro \ll 1$ and $E \ll 1$ the tangential component is brought to zero within an Ekman layer of non-dimensional thickness $(\nu/\Omega)^{\frac{1}{2}}$ which is set up on a timescale of order of the inertial time $(2\Omega)^{-1}$. Since this is shorter than any timescale considered herein, it may be assumed that the Ekman layer is set up instantaneously. This layer causes an Ekman-pumping contribution to the vertical velocity, and thus the lower boundary condition becomes

$$w^* = u^*\frac{\partial z^*}{\partial x^*} + v^*\frac{\partial z^*}{\partial y^*} + \frac{1}{2}\left(\frac{\nu}{\Omega}\right)^{\frac{1}{2}}\left(\frac{\partial v^*}{\partial x^*} - \frac{\partial u^*}{\partial y^*}\right) \quad \text{on} \quad z^* = h_0 f,$$

where the obstacle height is given by $h_0 f(x, y)$ and f has a maximum value of unity.

In terms of the non-dimensional variables,

$$w = uf_x + vf_y + \tfrac{1}{2}\gamma(v_x - u_y) \quad \text{on} \quad z = \delta f, \tag{2.4a}$$

$$w = -\tfrac{1}{2}\gamma(v_x - u_y) \quad \text{on} \quad z = 1, \tag{2.4b}$$

where $\gamma = (\nu/\Omega h_0^2)^{\frac{1}{2}}$ measures the ratio of the Ekman-layer thickness to the height of the obstacle.

In the following sections (2.2) and (2.4) are considered in the quasigeostrophic limit, $Ro \to 0$ with γ, λ and $S = \delta/Ro$ fixed.† The parameter S is the topographic parameter introduced by Hide (1961) and measures the importance of vortex stretching in the motion. In this limit (2.2*a*, *b*, *c*) give the geostrophic relations

$$u = -p_y, \quad v = p_x, \quad p_z = 0, \tag{2.5a, b, c}$$

and (2.2*d*) and (2.4) combine to give

$$w = S(1-z)\,\partial(p,f) + \gamma(\tfrac{1}{2}-z)\,S\nabla_1^2 p \tag{2.6}$$

and the field equation

$$\nabla_1^2 p_\tau + \partial(p, \nabla_1^2 p + Sf) = -\gamma S \nabla_1^2 p, \tag{2.7}$$

subject to the boundary conditions

$$p = 0 \quad \text{at} \quad \tau = 0 \quad \text{for each } x, y, \tag{2.8a}$$

$$p \to -y \quad \text{as} \quad x^2 + y^2 \to \infty \quad \text{for} \quad \tau > 0, \tag{2.8b}$$

where $\partial(p,) = p_x \partial_y - p_y \partial_x$. System (2.7), (2.8) is a form of the quasigeostrophic potential-vorticity equation given by Phillips (1963), discussed by Ingersoll (1969) and integrated numerically by James (1980).

For small S the perturbation to the oncoming flow is small. This corresponds to the 'fast' case of Huppert & Bryan (1976), and for inviscid flow (2.7) and (2.8) have the simple solution

$$p = -y + S[P(x,y) - P(x-\tau, y)] + O(S^2), \tag{2.9}$$

where

$$P(x,y) = \frac{1}{4\pi}\iint_{-\infty}^{\infty} \log[(x-\xi)^2 + (y-\eta)^2]\, f(\xi,\eta)\,\mathrm{d}\xi\,\mathrm{d}\eta$$

is the solution of $\nabla_1^2 P = -f$. The flow consists of an anticyclonic vortex above topography and an equal and opposite cyclonic vortex advected downstream at the free-stream velocity. James (1980) discusses the modification of this solution caused by Ekman pumping.

For large S the obstacle dominates the local flow field, and the relevant timescale is the topographic scale $h/2\Omega h_0$. In terms of the topographic time $t = 2\Omega h_0 t^*/h = S\tau$,

$$\nabla_1^2 p_t = -\partial(p,f) - \gamma \nabla_1^2 p - S^{-1}\partial(p, \nabla_1^2 p), \tag{2.10}$$

subject to the boundary conditions (2.8). The terms on the right in (2.10) describe the topographic generation of vorticity and its subsequent dissipation by Ekman pumping and advection by the perturbation field. Solutions of (2.10) for various obstacle shapes are discussed in the following sections.

Equation (2.10) is related to the linear initial-value problem for a sphere in a rotating flow considered by Stewartson (1953, 1967). Consider system (2.2) in the limit

† The parameter $H = Ro/\lambda$, introduced by Stewartson & Cheng (1979), measuring the ratio of fluid depth to the vertical scale of inertial waves, is thus zero. Vertical variations due to inertial waves are absent. Attention is confined to obstacles of small fractional height as this limit implies $h_0 \ll h$. Higher obstacles would also introduce vertical variations.

$\delta \to 0$ with $Ro = o(\delta)$, $E = o(\delta^2)$ and $\alpha = \delta/\lambda = h_0/l$, the obstacle slope, fixed. Then (2.2a, b) gives the geostrophic relations (2.5a, b) and the remaining equations become

$$p_z = -\alpha^2 w_t, \quad w_z = \nabla_1^2 p_t, \tag{2.11a, b}$$

subject to the boundary conditions

$$w = \partial(p,f) \quad (z = 0), \quad w = 0 \quad (z = 1). \tag{2.12a, b}$$

It follows from (2.11) that both w and p satisfy the inertial-wave equation

$$\alpha^2 \nabla_1^2 p_{tt} + p_{zz} = 0. \tag{2.13}$$

The solution of (2.11) and (2.12) is precisely the solution obtained by Stewartson (1967) by considering the inviscid linear equations (i.e. $Ro = 0$ and $E = 0$ in (2.2)), expressing the solution as an inverse Laplace transform and considering only the contributions from poles at the origin. Stewartson (1953, 1967) notes that this procedure is sufficient except in the neighbourhood of the circumscribing cylinder and on the surface of the obstacle. The inviscid linear form of (2.10) follows from (2.11) and (2.12) in the limit of vanishing obstacle slope, $\alpha \to 0$.

An alternative procedure for obtaining the inviscid linear form of (2.10) is to consider obstacles of small slope directly in (2.2) by taking the limit $\delta \to 0$, with $Ro = o(\delta)$, $E = o(\delta^2)$ and λ fixed. Then (2.2) gives the geostrophic relations (2.5) together with (2.11b) and the boundary conditions (2.12). Since w is a linear function of z, these may be combined to give precisely (2.10) with $\gamma = 0$ and $S^{-1} = 0$. The large-S limit of the quasigeostrophic potential-vorticity equation is equivalent to the small-slope limit of the linear starting-flow problem.

The simple form (2.10) is a viscously modified, nonlinear form of the equation for topographic Rossby waves considered by Rhines (1969). The simplification, which enables analytic progress to be made, follows from the separation of timescales chosen. In the present limit the ratios inertial period : topographic and viscous spin-up times : advection time are $1 : \delta^{-1} : Ro^{-1}$. For large S topographic waves cycle the obstacle many times before advection becomes important, whereas for small S the anticyclonic vortex is swept downstream before any significant rotation of the distribution can take place.

3. Axisymmetric obstacles

Provided $S \gg 1$, the final term in (2.10) is negligible outside regions of high vorticity gradients and may be neglected in determining the evolution of the flow for small t. This leaves a linear equation with non-constant coefficients for p, which may be simplified by introducing polar coordinates $(x, y) = (r\cos\theta, r\sin\theta)$ and considering axisymmetric topography, $f(x, y) = g(r)$. Then p satisfies

$$\nabla_1^2 p_t - r^{-1} g'(r)\, p_\theta = -\gamma \nabla_1^2 p, \tag{3.1}$$

$$\nabla_1^2 p = 0 \quad \text{at} \quad t = 0 \quad \text{for each } r, \theta, \tag{3.2a}$$

$$p \to -r\sin\theta \quad \text{as} \quad r \to \infty \quad \text{for} \quad t > 0. \tag{3.2b}$$

This system possesses a solution of the form

$$p = -r\sin\theta + \mathrm{Re}\,[F(r,t)\exp(\mathrm{i}\theta)], \tag{3.3}$$

provided

$$(\partial_t+\gamma)\,\mathscr{L}F-\mathrm{i}r^{-1}g'(r)\,F=-g'(r), \tag{3.4}$$

$$\mathscr{L}F=0 \quad \text{at} \quad t=0, \tag{3.5a}$$

$$F=o(1) \quad \text{as} \quad r\to\infty \quad \text{for} \quad t>0, \tag{3.5b}$$

where $\mathscr{L}F=F_{rr}+r^{-1}F_r-r^{-2}F$. Introducing the Laplace transform

$$\hat{F}(r,s)=\int_0^\infty \exp(-st)\,F(r,t)\,\mathrm{d}t$$

gives

$$(s+\gamma)\,\mathscr{L}\hat{F}-\mathrm{i}r^{-1}g'(r)\,\hat{F}=-s^{-1}g'(r), \tag{3.6}$$

$$\hat{F}=o(1) \quad \text{as} \quad r\to\infty. \tag{3.7}$$

In regions where the topography is flat, i.e. outside the support of g and above plateaux, (3.6) shows that the motion is irrotational, i.e. $\mathscr{L}F=0$. Moreover, at any point of discontinuity of g, the vorticity possesses a discontinuity of the same order as that of g'. Rhines (1969) discusses wavelike solutions of the inviscid form of (3.1), showing for isolated topography that the family of waves is countably infinite with independent discrete radial and azimuthal wavenumbers. Since solutions of the form (3.3) are required here, only waves with azimuthal wavenumber unity appear. More complicated upstream flows would force other azimuthal wavenumbers as, in the present case, would nonlinear interactions via the final term of (2.10). Hickie (1972) discusses steady solutions of (3.1). The form (3.3) implies that the circulation round the obstacle is zero for all time: positive and negative vorticity are generated in equal amounts. Steady viscous solutions in the limit $\gamma\to 0$ thus approach the zero-circulation solutions of Jacobs (1964) and Stewartson (1967).

A gross measure of the strength of the perturbation is given by the force exerted on the obstacle by the flow. This can be expressed as a drag F_X and a lift F_Y defined by

$$\int_{-\infty}^{\infty}\int_{-\infty}^{\infty} p^*\left(\frac{\partial f^*}{\partial x^*},\frac{\partial f^*}{\partial y^*}\right)\mathrm{d}x^*\,\mathrm{d}y^*=2\rho\Omega U h_0 l^2 V(F_X,F_Y), \tag{3.8}$$

where V is the non-dimensional volume of the obstacle and the forces are non-dimensionalized on the Coriolis force on a volume V of the fluid. These may be combined to give

$$F_X-\mathrm{i}F_Y=-\mathrm{i}+\frac{\pi}{V}\int_0^\infty F(r,t)\,g'(r)\,r\,\mathrm{d}r, \tag{3.9}$$

and its equivalent form in terms of the transform $\hat{F}$.

4. Right-circular cylinder

Consider a cylinder, for which g is unity for $r<1$ and zero otherwise. Since g' vanishes for $r\neq 1$, the motion is irrotational for $r\neq 1$. Hence

$$F=\begin{cases} A(t)\,r & \text{if} \quad r<1, \qquad (4.1a)\\ A(t)\,r^{-1} & \text{if} \quad r>1. \qquad (4.1b)\end{cases}$$

Integrating (3.6) from $1-\epsilon$ to $1+\epsilon$ for $0<\epsilon\ll 1$ gives

$$(s+\gamma)\,[F_r]=[g]\{\mathrm{i}F(1)-s\}, \tag{4.2}$$

where $[g]$ denotes the jump in g at $r = 1$. Combining (4.1) and (4.2) gives

$$A(t) = \frac{1-\exp[(-\gamma+\frac{1}{2}\mathrm{i})t]}{\mathrm{i}-2\gamma}. \tag{4.3}$$

The flow consists of unsteady irrotational motion away from the edge of the cylinder and a shear layer at the cylinder boundary which rotates with non-dimensional period 4π, i.e. with period $4\pi h/2\Omega h_0$. Viscosity causes this motion to spin down with a non-dimensional e-folding time of γ^{-1}, i.e. dimensionally $h(\Omega/\nu)^{\frac{1}{2}}(2\Omega)^{-1}$, the viscous spin-up time. The steady state is given by

$$p = \begin{cases} \dfrac{-2\gamma r(\cos\theta + 2\gamma\sin\theta)}{1+4\gamma^2} & \text{if} \quad r < 1, \qquad (4.4a) \\ -r\sin\theta + \dfrac{\sin\theta - 2\gamma\cos\theta}{r(1+4\gamma^2)} & \text{if} \quad r > 1. \qquad (4.4b) \end{cases}$$

This is the solution given by Hickie (1972).

A gross measure of the decay of the motion is given by considering the force exerted on the cylinder by the flow. From (3.9), the drag F_X and lift F_Y are given by

$$F_X - \mathrm{i}F_Y = -\mathrm{i} - F(1,t) = -\mathrm{i} - A(t). \tag{4.5}$$

The drag oscillates with frequency $\frac{1}{2}$ and decaying amplitude about a mean value of $2\gamma/(1+4\gamma^2)$, and the lift oscillates similarly about the value $4\gamma^2/(1+4\gamma^2)$. This behaviour models the numerical results presented in figure 8 of James (1980). The comparison is discussed further in §5.

For inviscid flow, $\gamma = 0$, the drag and lift do not decay, and the stream function has the simple form

$$p = \begin{cases} -r\sin(\theta+\frac{1}{2}t) & \text{if} \quad r < 1, \qquad (4.6a) \\ -(r-r^{-1})\sin\theta - r^{-1}\sin(\theta+\frac{1}{2}t) & \text{if} \quad r > 1. \qquad (4.6b) \end{cases}$$

The flow in $r > 1$ consists of the superposition of steady irrotational flow past a cylinder, i.e. a uniform stream and a dipole fixed at the origin and directed in the negative x-direction, and a dipole of the same strength at the origin rotating with constant angular velocity $\frac{1}{2}$. The steady flow contributes a constant unit value to the lift and the rotating dipole the oscillatory contribution to both the drag and the lift. Figure 1 gives streamline patterns at quarter-period intervals.

It is perhaps more informative to consider particle paths for the inviscid motion, which follow from integrating

$$\left(\frac{\mathrm{d}x^*}{\mathrm{d}t^*}, \frac{\mathrm{d}y^*}{\mathrm{d}t^*}\right) = (u^*, v^*), \quad \text{i.e.} \quad \left(\frac{\mathrm{d}x}{\mathrm{d}t}, \frac{\mathrm{d}y}{\mathrm{d}t}\right) = S^{-1}(-p_y, p_x).$$

For $r < 1$ this gives $(x,y) = (x_0 + 2S^{-1}\sin\frac{1}{2}t,\ y_0 + 2S^{-1}[\cos\frac{1}{2}t - 1])$. The particles describe circles of radius $2S^{-1} \ll 1$ in time $t = 4\pi$. For $r > 1$ the paths are more complicated but, in general, particles originating at $x = -\infty$ pass to $x = +\infty$. Figure 2 shows particle paths for the cylinder for $S = 10$, displaying asymmetry about the line $y = 0$ due to the presence of topographic waves. The average of the inviscid flow over one period gives irrotational flow past a cylinder for $r > 1$ and stagnant flow for $r < 1$. This is the steady symmetric flow described by Stewartson (1967).

The presence of a vortex sheet at $r = 1$ means that in the neighbourhood of this region either the neglected nonlinear terms in (2.10) or horizontal diffusion will be important, and the flow may also have a more complicated vertical structure. The

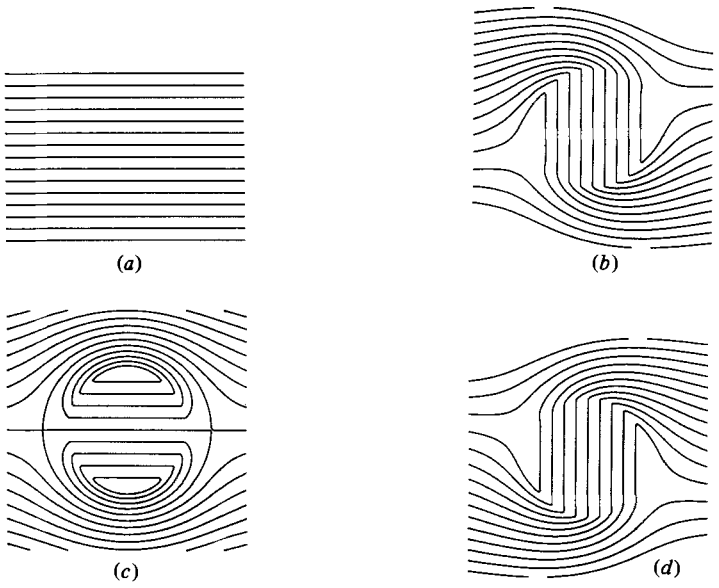

FIGURE 1. The stream function, of period $4\pi h/2\Omega h_0$, above a right-circular cylinder at quarter-period intervals: (*a*) $t = 0$; (*b*) π; (*c*) 2π; (*d*) 3π. The undisturbed flow is from left to right and the streamline interval is 0.2.

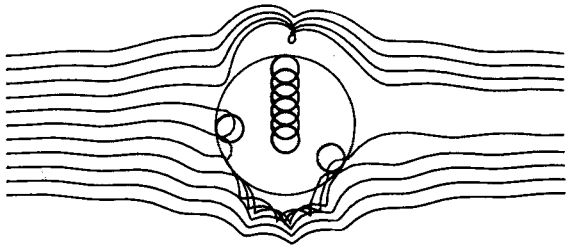

FIGURE 2. Particle paths over a right-circular cylinder for $S = 10$. Particles released on the left (upstream) pass asymmetrically downstream, avoiding the cylinder. Particles released above the centreline of the cylinder ($x = 0$) move in phase round circular paths. In this example two particles originating upstream are captured over the cylinder, whilst others pass through the shear layer before moving downstream.

vortex sheet is present for all $t > 0$. For obstacles whose height is a continuous function of r but whose slope is discontinuous, a similar sheet forms for $t \gg 1$ as shown in the following example.

5. Paraboloid

Consider the smoother obstacle given by the paraboloid,

$$g(r) = \begin{cases} \frac{1}{2}(1-r^2) & \text{if} \quad r < 1, \qquad (5.1a) \\ 0 & \text{if} \quad r > 1. \qquad (5.1b) \end{cases}$$

Since the motion is irrotational for $r > 1$, F is of the form (4.1*b*) there. Requiring the continuity of F and its first derivative at $r = 1$ gives the boundary condition

$$\hat{F}_r(1) + \hat{F}(1) = 0. \qquad (5.2)$$

The solution of (3.6) with g given by (5.1), subject to (5.2), can be written in terms of Bessel functions of the first kind,

$$\hat{F} = \frac{\mathrm{i}}{s}\left[\frac{2J_1(\mu r)}{\mu J_0(\mu)} - r\right], \tag{5.3}$$

where $\mu = (\mathrm{i}/s+\gamma)^{\frac{1}{2}}$. Since F is an even function of μ, there is no ambiguity in the sign of μ nor are the usual branch cuts associated with square roots present in the Bromwich inversion integral. The singularities of the integrand consist of simple poles at $s = 0$ and $s = -\gamma + \mathrm{i}/j_n^2$, $n = 1, 2, \ldots$, where the j_n are the zeroes of J_0 in ascending order. By choosing the limit of inversion contours omitting circles of radius $\epsilon_n = 1/j_n j_{n+1}$ about the accumulation point $s = \gamma$, and writing $\mu_0 = (\mathrm{i}/\gamma)^{\frac{1}{2}}$, it follows that

$$p = \begin{cases} \mathrm{Re}\left[\dfrac{2\mathrm{i}\exp(\mathrm{i}\theta)J_1(\mu_0 r)}{\mu_0 J_0(\mu_0)}\right] + 4\exp(-\gamma t)\sum_1^\infty \mathrm{Re}\left\{\dfrac{\exp[\mathrm{i}(\theta + t/j_n^2)]}{\mathrm{i}-\gamma j_n^2}\right\}\dfrac{J_1(j_n r)}{j_n^2 J_1(j_n)} & \\ \qquad\qquad \text{if} \quad r < 1, & (5.4a) \\ -r\sin\theta + \dfrac{4}{r}\exp(-\gamma t)\sum_1^\infty j_n^{-2}\,\mathrm{Re}\left\{\dfrac{\exp[\mathrm{i}(\theta + t/j_n^2)]}{\mathrm{i}-\gamma j_n^2}\right\} & \text{if} \quad r > 1. \quad (5.4b) \end{cases}$$

The uniform convergence of this series for $0 \leqslant r \leqslant 1-\epsilon$ for $\epsilon > 0$ follows from the discussion of Fourier–Bessel series in Watson (1944, chap. 18). An alternative form of (5.4), which enables the stream function to be evaluated without using Bessel functions of complex argument, can be obtained by constructing a Dini series for $J_1(\mu_0 r)$ (Watson 1944, chap. 18). This gives

$$p = \begin{cases} -r\sin\theta + 4\sum_1^\infty A_n(\theta, t)\dfrac{J_1(j_n r)}{j_n^2 J_1(j_n)} & \text{if} \quad r < 1, \quad (5.5a) \\ -r\sin\theta + \dfrac{4}{r}\sum_1^\infty \dfrac{A_n(\theta, t)}{j_n^2} & \text{if} \quad r > 1, \quad (5.5b) \end{cases}$$

introducing, for brevity, the notation

$$A_n(\theta, t) = \mathrm{Re}\left\{\frac{\exp(\mathrm{i}\theta) - \exp(\mathrm{i}\theta + \mathrm{i}t/j_n^2 - \gamma t)}{\mathrm{i}-\gamma j_n^2}\right\}. \tag{5.6}$$

Form (5.5) shows more clearly that the flow set up instantaneously at $t = 0$ is uniform. The solution consists of viscously damped topographic Rossby waves of azimuthal wavenumber unity cycling clockwise round the obstacle, forcing outside the circumscribing cylinder an unsteady irrotational flow whose strength decays inversely with distance from the obstacle. As $t \to \infty$, with $\gamma > 0$, the solution decays to that given by Hickie (1972). The vorticity of the flow, which vanishes in $r > 1$, is given in $r < 1$

$$\nabla_1^2 p = -4\sum_1^\infty A_n(\theta, t)\frac{J_1(j_n r)}{J_1(j_n)}. \tag{5.7}$$

Figure 3 gives the steady-state stream-function and vorticity distributions for various γ. For small γ, i.e. large μ_0, replacing the Bessel function in (5.4) by its asymptotic form gives (Hickie 1972)

$$\nabla_1^2 p \to r^{-\frac{1}{2}}\exp[-(1-r)(2\gamma)^{\frac{1}{2}}]\cos[(1-r)(2\gamma)^{-\frac{1}{2}} + \theta - \tfrac{1}{4}\pi]. \tag{5.8}$$

The distribution decays exponentially outside a region of thickness $\gamma^{\frac{1}{2}}$ near $r = 1$ and vanishes on the spiral

$$(2\gamma)^{-\frac{1}{2}}(1-r) + \theta - \tfrac{1}{4}\pi = \pm\tfrac{1}{2}\pi, \tag{5.9}$$

as can be seen in figure 3.

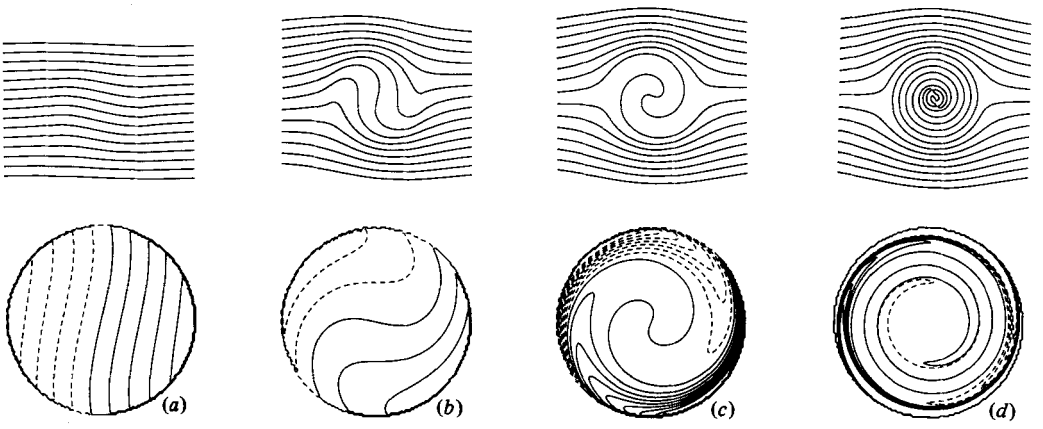

FIGURE 3. The steady-state stream function and vorticity for slow flow over a paraboloid as functions of $\gamma = (\nu/\Omega h_0^2)^{\frac{1}{2}}$, the ratio of Ekman-layer thickness to obstacle height: (*a*) $\gamma = 1$; (*b*) 0.1; (*c*) 0.01; (*d*) 0.001. For small γ the vorticity is exponentially small outside a region of thickness $\gamma^{\frac{1}{2}}$ near $r = 1$. Vorticity patterns are shown at twice the horizontal scale of streamline patterns, and contours of negative vorticity are dotted. The streamline interval is 0.2 and the vorticity contour interval is 2, except in (*a*) where it is 0.2.

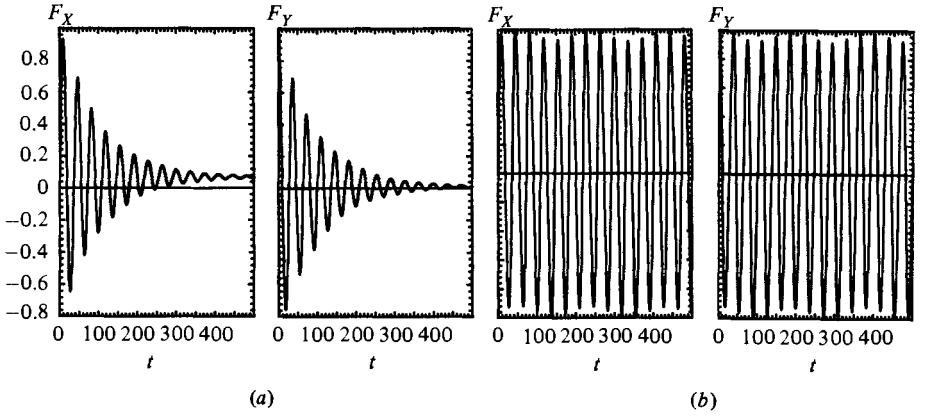

FIGURE 4. The non-dimensional drag F_X and lift F_Y for the paraboloid as a function of the topographic time t. The force oscillates on a timescale of order $h/2\Omega h_0$ and decays with e-folding time equal to the viscous spin-up time $h(\nu/\Omega)^{-\frac{1}{2}}(2\Omega)^{-1}$. (*a*) Viscous flow, $\gamma = 0.01$; (*b*) inviscid flow.

The force on the obstacle follows from (3.9) as

$$F_X - \mathrm{i}F_Y = -\mathrm{i} - 32\sum_1^\infty \frac{1-\exp(-\gamma t + \mathrm{i}t/j_n^2)}{j_n^4[\mathrm{i}-\gamma j_n^2]}. \tag{5.10}$$

Figure 4(*a*) presents the non-dimensional lift and drag forces on the paraboloid for $\gamma = 0.01$ and, as for the cylinder, shows similar behaviour to figure 8 of James (1980), in which his $k = \gamma S = 0.05$ and $S = 25$, giving $\gamma = 0.002$ and his timescale $\tau = S^{-1}t = 0.04t$. The drag decays more rapidly in James' case owing to the destruction of high vorticity gradients by horizontal diffusion and nonlinear effects. The asymptotic value of the drag is given by

$$F_X = 32\gamma\sum_1^\infty [j_n^2(1+\gamma^2 j_n^4)]^{-1}. \tag{5.11}$$

It is proportional to γ for small γ, i.e. in James' (1980) notation the drag is constant on lines where S is proportional to k. This can be seen to approximate closely the numerical results for $S > 10$ presented in figure 7 of James (1980). For arbitrary topography $f(x, y)$ the small-γ result follows by linearizing the flow about the upstream conditions and gives

$$F_X = \gamma^2 \int\int_{-\infty}^{\infty} \frac{|\hat{f}|^2}{(k^2+l^2)(\gamma+ik)} \,dk\,dl, \tag{5.12}$$

when

$$\hat{f}(k,l) = \int\int_{-\infty}^{\infty} f(x,y) \exp(ikx+ily)\,dy\,dl.$$

This expression is valid at large time for $S \gg 1$. The lift is of order γ^2, as for the cylinder.

The drag in inviscid flow is given, from (5.10), by

$$F_X = 32 \sum_{1}^{\infty} \frac{\sin(t/j_n^2)}{j_n^4}. \tag{5.13}$$

Since $\Sigma_1^\infty j_n^{-4} = \frac{1}{32}$ (Watson 1944, chap. 14) and $j_1^{-4} = 0.030$, the value of F_X deviates from the first term in (5.13) by less than 4 % of its maximum value. Hence the force on the cylinder is due almost entirely to the lowest mode present. As in the case of a cylinder, the stream function in $r > 1$ may be approximated by a fixed and a rotating dipole at the origin. The period of rotation is approximately $2\pi j_1^2 = 36.3$. Figure 4(*b*) gives the inviscid drag and lift for the paraboloid.

Figure 5 gives streamline patterns and vorticity distributions for the inviscid flow. The patterns were obtained by two distinct direct methods: first, by summing 100 terms of the series and using an asymptotic form for the tail, and, secondly, by expanding the vorticity as a series of Chebyshev polynomials with time-dependent coefficients and solving the resulting ordinary differential equations for the coefficients using a variable-step, variable-order Adams' method. The two sets of results were graphically indistinguishable. At small and moderate values of t the vorticity pattern closely mirrors the pattern of the steady viscous solutions of figure 3 at values of γ equal to $1/t$. This occurs since γ appears in the steady solution in the same manner as s in the transform of the unsteady solution. The analogy is not valid at large times, as s cannot be precisely identified with $1/t$. After an initial transient phase the stream function settles into approximately periodic flow. The streamline patterns at intervals of $\frac{1}{2}\pi j_1^2$ at large time, given in figures 5(*e–h*), are closely comparable to the exactly periodic flow of the cylinder. The largest discrepancy occurs at those times when the lowest mode is absent and the flow near the obstacle is dominated by the weaker second mode. A more complete asymptotic analysis (presented in the Appendix) of the structure of the solution confirms that the dominant contribution to the stream function at large time comes from the lowest topographic modes, with the contribution from the neighbourhood of $s = 0$ decaying as $t^{-\frac{1}{2}}$.

This is not the case with the vorticity distribution. The small-time behaviour follows by solving the governing equations as a power series in time after Grace (1927) or by evaluating the inverse Laplace transform by expanding the integrand as a power series of inverse powers of s. Both give

$$\nabla_1^2 p = y(r^2-2)(\tfrac{1}{4}t)^2 - y(r^6-12r^4+48r^2-76)(\tfrac{1}{4}t)^4/864 + \ldots$$
$$+ xt - x(r^2-3)(\tfrac{1}{4}t)^3/18 + \ldots \tag{5.14}$$

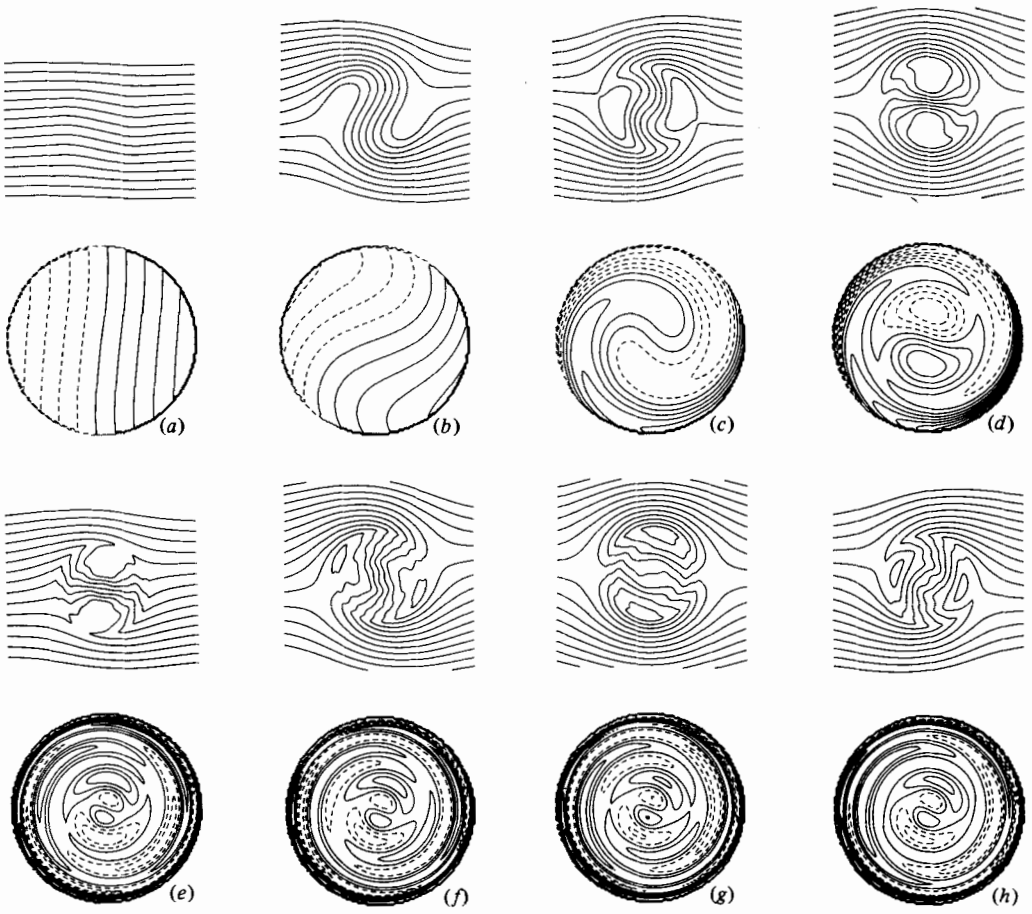

FIGURE 5. The stream function and vorticity distributions over a paraboloid as functions of the topographic time $t = 2\Omega h_0 t^*/h$: (*a*) $t = 1$; (*b*) 10; (*c*) 100; (*d*) 200; (*e*) 2000; (*f*) 2009; (*g*) 2018; (*h*) 2027. The vorticity contour interval is 0.2 in (*a*), 2 in (*b*) 4 in (*c*) and 8 in the remainder.

Initially the vorticity is proportional to x, i.e. positive on the downstream half of the obstacle and negative on the upstream half, as noted from vortex-compression arguments by Huppert & Bryan (1976). As higher-order terms become important, the positive and negative vorticities interlace. At larger times it may be noted that the line of zero vorticity originates at $\theta = \frac{1}{4}\pi$ or $\frac{3}{4}\pi$ and spirals in towards the origin. This follows from the asymptotic form (see Appendix) for the vorticity at large time (in $0 < r < 1$):

$$\nabla_1^2 p = (\tfrac{8}{3}\pi r)^{\frac{1}{2}}(1-r)^{-\frac{2}{3}}(2t)^{\frac{1}{6}}\cos[\tfrac{3}{2}(1-r)^{\frac{2}{3}}(2t)^{\frac{1}{3}}+\theta+\tfrac{1}{4}\pi], \tag{5.15}$$

which vanishes on the spirals given by

$$\theta+\tfrac{3}{2}(1-r)^{\frac{2}{3}}(2t)^{\frac{1}{3}}+\tfrac{1}{4}\pi = \pm\tfrac{1}{2}\pi,$$

whose number of cycles of the origin increases as $t^{\frac{1}{3}}$. In the neighbourhood of the origin the vorticity vanishes according to (5.4). The patterns in figures 5(*e–h*) show the vorticity distribution in the neighbourhood of the column boundary varying little over the topographic period, with the lower modes, which affect the stream function, being important away from $r = 1$ and causing the distribution to rotate clockwise

in $r < 1$ with approximate period $2\pi j_1^2$. With increasingly large t the vorticity becomes more and more convoluted, increasing at each $0 < r < 1$ as $t^{\frac{1}{6}}$. At this stage of the evolution of the flow the presence of high gradients mean that either horizontal diffusion, nonlinearity or vertical variations become important. These effects are discussed briefly in §6.

6. Discussion

The initial-value problem for rotating flow over topography of height small compared with its horizontal scale has been considered. The starting flow excites topographic Rossby waves, which cycle clockwise round the obstacle with almost constant frequency given by the lowest mode of azimuthal wavenumber unity possible above the obstacle. The period of oscillation for a general obstacle in uniform motion is thus estimated by the smallest eigenvalue for the azimuthal mode-one problem. When Ekman pumping is present these waves decay on the viscous spin-up time to leave the steady solutions discussed by Hickie (1972). In inviscid flow the wave motion is undamped, causing lift and drag forces on the obstacle which oscillate with undiminishing amplitude approximately equal to the Coriolis force on a volume of fluid equal to that of the obstacle. For a right-circular cylinder a vortex sheet is present from the start of the motion, whereas for a paraboloid this sheet forms when topographic waves have cycled the obstacle many times. By this time the vorticity is increasing without bound everywhere above the obstacle, and the present analysis is invalid. Which neglected effect first becomes important depends on the relative magnitudes of the small parameters measuring the obstacle slope α, the inverse S^{-1} of the topographic forcing, and the horizontal diffusion E. Above regions of greater slope, such as the walls of a right cylinder or the sphere considered by Stewartson (1967), or for obstacles of greater fractional height δ, the topographic period decreases towards the inertial period, and the motion at the boundary of the column is no longer constrained to be two-dimensional. For smaller values of the topographic parameter S, i.e. larger values of S^{-1}, solutions of (2.10) are no longer monochromatic. Nonlinear interactions force higher-azimuthal-wavenumber perturbations to the flow. If horizontal diffusion is the largest of the small effects then at large values of the topographic time the flow could become steady, with the system of vertical shear layers discussed by Jacobs (1964) and Stewartson (1966) present at the boundary of the column and stagnant flow inside.

The present solutions show that, in the limit $S \to \infty$, the steady flow determined by Ekman pumping in the limit of vanishing viscosity is the zero-circulation flow of Jacobs (1964) and Stewartson (1967), and not the single-stagnation-point flow that is the $S \to \infty$ limit of Ingersoll's (1969) solution. The difference appears to lie in the order of taking the limits $S \to \infty$ and $\gamma \to 0$. The present solution has $\gamma S = E_h^{\frac{1}{2}}/Ro \to \infty$, where $E_h = \nu/2\Omega h^2$ is the Ekman number based on fluid depth and γS measures the ratio of advection time to viscous spin-up time. Ingersoll's derivation applies to less-viscous flows where $E_h^{\frac{1}{2}}/Ro \to 0$. The solutions also illustrate, for obstacles of small slope, that the presence of topographic waves causes the order of taking the limits $\gamma \to 0$, $t \to \infty$ to be important. In particular, the force on an obstacle in inviscid flow has no steady long-time value.

The flows can be regarded as due to forcing of Rossby waves along an escarpment by a uniform stream (Smith 1971; Rhines 1969; Longuet-Higgins 1968). This leads to the conjecture that the boundary of a Taylor column on a smooth distributed obstacle is that line on which the obstacle gradient has a turning point (Smith 1971),

i.e. a point of inflection of the obstacle profile. As noted from (3.6) the vorticity has the same order of continuity as the slope of the obstacle, i.e. the restoring mechanism for the topographic waves. Hence the singularity at the edge of the Taylor column is weaker for obstacles of continuous slope (since the first three derivatives of the stream function are continuous) although the oscillatory behaviour of the flow is still present. The flow above such obstacles will be considered elsewhere.

The present analysis extends directly to horizontally sheared oncoming flow, predicting dominant disturbances of azimuthal wavenumber 2 in linearly sheared flow and higher-order disturbances in variably sheared flow. The extension to stratified flow is also direct.

I am indebted to Dr S. N. Brown for providing arguments which led to the evaluations in the Appendix.

This paper reports work presented at the 5th UK Geophysical Assembly, Cambridge, 1981.

Appendix. Asymptotic forms for the inviscid stream function and vorticity

The stream function in $r < 1$ is given by the integral

$$I = -\frac{\mathrm{i}}{\pi}\int \frac{\mu J_1(\mu r)}{J_0(\mu)} \exp(st)\,\mathrm{d}s, \tag{A 1}$$

where, as noted previously, there are no branch cuts present and the small-t behaviour may be obtained by expanding I as a power series in s^{-1}. The path of integration lies to the right of the poles of the integrand (shown as crosses in figure 6) and a suitable path C_0 is shown dotted there. Suppose the path is distorted to C_1, shown by the solid line in figure 6. It will be shown below that dominant contributions to I come from saddle points at A and B (to be determined) and from those poles lying to the right of C_1.

Consider the evaluation of I round any small circle centred on the origin. The argument of s increases by 2π on the path. Take $-\frac{3}{2}\pi < \arg s < \frac{1}{2}\pi$ for definiteness. This choice gives $0 < \arg\mu < \pi$. (Note that, since μ enters solely as μ^2, which square root is chosen is immaterial.) Now for $|s| \ll 1$, i.e. $|\mu| \gg 1$,

$$\frac{J_1(\mu r)}{J_0(\mu)} \sim \frac{r^{-\frac{1}{2}}[\exp(\mathrm{i}\mu r - \frac{3}{4}\pi\mathrm{i}) + \exp(-\mathrm{i}\mu r + \frac{3}{4}\pi\mathrm{i})]}{\exp(\mathrm{i}\mu - \frac{1}{4}\pi\mathrm{i}) + \exp(-\mathrm{i}\mu + \frac{1}{4}\pi\mathrm{i})} \sim \mathrm{i}r^{-\frac{1}{2}}\exp(\mathrm{i}\mu\xi), \tag{A 2}$$

since $\mathrm{Im}\,\mu > 0$, where $1 > \xi = 1 - r > 0$. Thus (A 1) reduces to

$$I \sim \frac{1}{\pi r^{\frac{1}{2}}}\int \exp[\mathrm{i}E(\mu)]\,\mu\,\mathrm{d}s, \tag{A 3}$$

where $E(\mu) = \mu^2\xi + t/\mu$. Saddle points of E occur where $\mu = (2t/\xi)^{\frac{1}{3}}, (2t/\xi)^{\frac{1}{3}}\exp(\pm\frac{2}{3}\pi\mathrm{i})$. The root with argument $-\frac{2}{3}\pi\mathrm{i}$ does not lie in the range of $\arg\mu$ under consideration. The root with argument $\frac{2}{3}\pi\mathrm{i}$ corresponds to the point $s = (\xi/2t)^{\frac{2}{3}}\exp(-\frac{5}{6}\pi\mathrm{i})$. Identify this point with B, noting that, as $t \to \infty$, B becomes arbitrarily close to the origin. A standard analysis gives the steepest-descent path through B as making an angle $\frac{1}{12}\pi$ with the $\mathrm{Re}\,s$ axis as shown in figure 6, and contributing to I a term

$$\left(\frac{4\pi}{3rt}\right)^{\frac{1}{2}}\exp[\tfrac{3}{2}\xi^{\frac{2}{3}}(2t)^{\frac{1}{3}}\exp(-\tfrac{5}{6}\pi\mathrm{i}) + \tfrac{7}{12}\pi\mathrm{i}]. \tag{A 4}$$

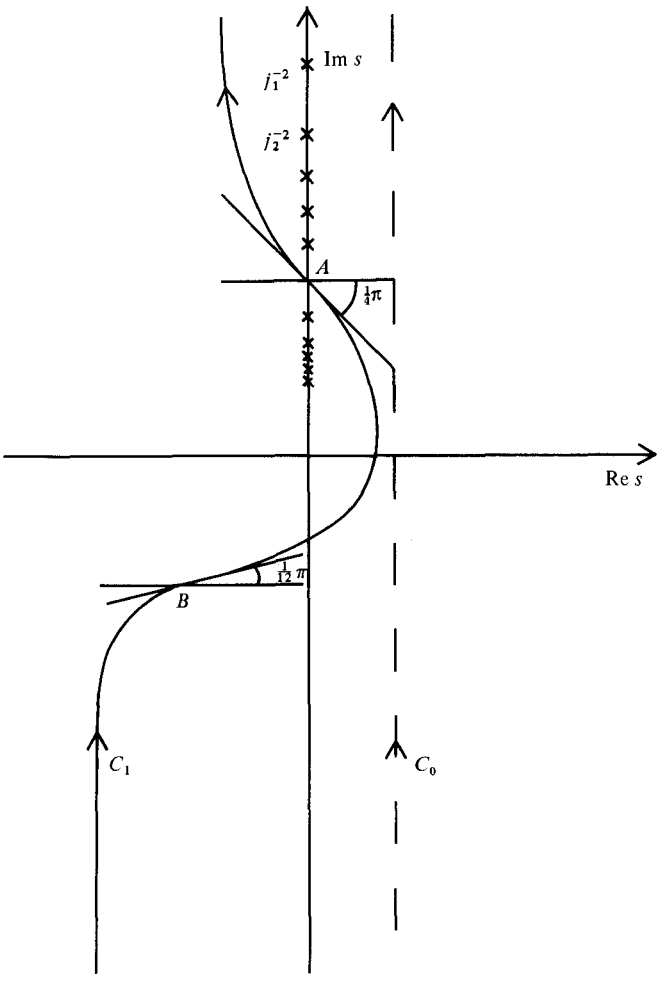

FIGURE 6. The integration paths for the evaluation of the inverse Laplace integral for the stream function and vorticity over a paraboloid. Poles of the integrand are marked by crosses, and the steepest-descent path through saddle points A and B is given by the solid line.

This term decays exponentially away from a region of thickness $t^{-\frac{1}{2}}$ near $r = 1$ and decays as $t^{-\frac{1}{2}}$ within this region.

It remains to consider the saddle point of E at $\mu = (2t/\xi)^{\frac{1}{3}}$. Reduction (A 2) is not valid for real μr. Hence to consider this contribution for real μ suppose ξ is complex, $\xi = \xi_r + i\xi_i$, where $\xi_i < 0$ and $|\xi_i/\xi_r| \ll 1$. This gives $\operatorname{Im} r > 0$, and reduction (A 2) is then valid not only for $\operatorname{Im}\mu > 0$ but also for $\operatorname{Im}\mu = 0$. The stationary point of E is displaced into $\operatorname{Im}\mu > 0$, corresponding, to lowest order in ξ_i, to $s = i(\xi/2t)^{\frac{2}{3}}$, and can be identified with A in figure 6. The steepest-descent path through A makes an angle $\frac{1}{4}\pi$ with the Re s axis as illustrated in figure 6, and contributes to I a term

$$\left(\frac{4\pi}{3rt}\right)^{\frac{1}{2}} \exp\left[\tfrac{3}{2}i\xi^{\frac{2}{3}}(2t)^{\frac{1}{3}} + \tfrac{1}{4}\pi i\right]. \tag{A 5}$$

Since ξ has negative imaginary part this term is exponentially large at large t, giving the dominant contribution near A. As $\xi_i \to 0$, the term remains the dominant saddle

point outside the shear layer near $r = 1$, decaying only algebraically, as $t^{-\frac{1}{2}}$, away from the region $1-r \sim t^{\frac{1}{2}}$. Nevertheless, its contribution is negligible at large time in comparison with those from the poles, which are order unity for all t. As noted in §5, drag considerations show the largest of the pole contributions to come from that at $s = \mathrm{i}/j_1^2$.

The vorticity is given by the integral

$$I = -\frac{1}{\pi}\int \frac{\mu J_1(\mu r)}{sJ_0(\mu)} \exp(st)\,\mathrm{d}s. \tag{A 6}$$

The same considerations apply to the choice of path, but now the contribution from B is given by

$$\left(\frac{8\pi}{3r}\right)^{\frac{1}{2}} (2t)^{\frac{1}{6}} \xi^{-\frac{2}{3}} \exp\left[\tfrac{3}{2}\xi^2 (2t)^{\frac{1}{3}} \exp\left(-\tfrac{5}{6}\pi\mathrm{i}\right) + \tfrac{11}{12}\pi\mathrm{i}\right)], \tag{A 7}$$

that from A by

$$\left(\frac{8\pi}{3r}\right)^{\frac{1}{2}} (2t)^{\frac{1}{6}} \xi^{-\frac{2}{3}} \exp\left[\tfrac{1}{2}\mathrm{i}\xi^2 (2t)^{\frac{1}{3}} + \tfrac{1}{4}\pi\mathrm{i}\right], \tag{A 8}$$

whilst those from the poles remain of order unity. Thus the order-one contributions from the poles are dominated at large time by the term (A 8), and the vorticity grows as $t^{\frac{1}{6}}$ everywhere except within a region of thickness $t^{-\frac{1}{2}}$ of $r = 1$ in which it grows as $t^{\frac{1}{2}}$.

REFERENCES

Batchelor, G. K. 1967 *An Introduction to Fluid Dynamics.* Cambridge University Press.

Cheng, H. K. 1977 On inertial wave and flow structure at low Rossby number. *Z. angew. Math. Phys.* **28**, 753–769.

Cheng, H. K. & Johnson, E. R. 1982 Inertial waves above an obstacle in an unbounded, rapidly rotating fluid. *Proc. R. Soc. Lond.* A **383**, 71–87.

Grace, S. F. 1927 On the motion of a sphere in a rotating liquid. *Proc. R. Soc. Lond.* A **133**, 46–77.

Hickie, B. P. 1972 Taylor columns for small Rossby numbers. In *Proc. GFD Summer School, Woods Hole Oceanographic Institute*, vol. II, pp. 29–39.

Hide, R. 1961 Origin of Jupiter's Great Red Spot. *Nature* **190**, 895–896.

Hide, R., Ibbetson, A. & Lighthill, M. J. 1968 On slow transverse flow past obstacles in a rapidly rotating fluid. *J. Fluid Mech.* **32**, 251–272.

Huppert, H. E. 1975 Some remarks on the initiation of inertial Taylor columns. *J. Fluid Mech.* **67**, 397–412.

Huppert, H. E. & Bryan, K. 1976 Topographically generated eddies. *Deep-Sea Res.* **23**, 655–679.

Ingersoll, A. P. 1969 Inertial Taylor columns and Jupiter's Great Red Spot. *J. Atmos. Sci.* **26**, 744–752.

Jacobs, S. J. 1964 The Taylor column problem. *J. Fluid Mech.* **20**, 581–591.

James, I. N. 1980 The forces due to geostrophic flow over shallow topography. *Geophys. Astrophys. Fluid Dyn.* **14**, 225.

Johnson, E. R. 1978 Trapped vortices in rotating flow. *J. Fluid Mech.* **86**, 209–224.

Johnson, E. R. 1982 The effects of obstacle shape and viscosity in deep rotating flow over finite-height topography. *J. Fluid Mech.* **120**, 359–383.

Longuet-Higgins, M. S. 1968 Double Kelvin waves with continuous depth profiles. *J. Fluid Mech.* **34**, 49–80.

Mason, P. J. & Sykes, R. I. 1981 A numerical study of rapidly rotating flow over surface mounted obstacles. *J. Fluid Mech.* **111**, 175–195.

Phillips, N. A. 1963 Geostrophic motion. *Rev. Geophys.* **1**, 123–176.

Rhines, P. B. 1969 Slow oscillations in an ocean of varying depth. Part 2. Islands and seamounts. *J. Fluid Mech.* **37**, 191–205.

SMITH, R. 1971 The ray paths of topographic Rossby waves. *Deep-Sea Res.* **18**, 477–483.

STEWARTSON, K. 1953 On the slow motion of an ellipsoid in a rotating fluid. *Q. J. Mech. Appl. Maths* **6**, 141–162.

STEWARTSON, K. 1966 On almost rigid rotations. Part 2. *J. Fluid Mech.* **26**, 131–144.

STEWARTSON, K. 1967 On the slow transverse motion of a sphere through a rotating fluid. *J. Fluid Mech.* **30**, 357–369.

STEWARTSON, K. & CHENG, H. K. 1979 On the structure of inertial waves produced by an obstacle in a deep, rotating container. *J. Fluid Mech.* **91**, 415–432.

TAYLOR, G. I. 1923 Experiments on the motion of solid bodies in rotating fluids. *Proc. R. Soc. Lond.* A **104**, 213–218.

WATSON, G. N. 1944 *Theory of Bessel Functions*, 2nd ed. Cambridge University Press.